

Theory of chirped photonic crystals in biological broadband reflectors

Caleb Q. Cook^{1,2,*} and Ariel Amir^{3,†}

¹*Department of Physics, Harvard University, Cambridge, Massachusetts 02138, USA*

²*Perimeter Institute for Theoretical Physics, Waterloo, Ontario N2J 2Y5, Canada*

³*School of Engineering and Applied Sciences, Harvard University, Cambridge, Massachusetts 02138, USA*

(Dated: May 23, 2017)

One-dimensional photonic crystals with slowly varying, i.e. ‘chirped’, lattice period are responsible for broadband light reflectance in many diverse biological contexts, ranging from the shiny coatings of various beetles to the eyes of certain butterflies. We present a quantum scattering analogy for light reflection from these adiabatically chirped photonic crystals (ACPCs) and apply a WKB-type approximation to obtain a closed-form expression for the reflectance. From this expression we infer several design principles, including a differential equation for the chirp pattern required to elicit a given reflectance spectrum and the minimal number of bilayers required to exceed a desired reflectance threshold. Comparison of the number of bilayers found in ACPCs throughout nature and our predicted minimal required number also gives a quantitative measure of the optimality of chirped biological reflectors. Together these results elucidate the design principles of chirped reflectors in nature and their possible application to future optical technologies.

Many of the brilliant colors throughout nature are produced via the interaction of light and microscopic structures, a phenomenon known as structural coloration [1–3]. In particular, certain species of beetles, butterflies, birds, spiders, and fish take advantage of structural color phenomena to achieve their striking appearance [4–7]. In many of these cases color arises even in the absence of pigments through the layered application of materials with differing refractive indices, structurally arranged so as to yield the desired color via light interference.

Perhaps the simplest such structure is a one-dimensional photonic crystal, i.e. a stack of dielectric slabs with alternating high and low refractive indices whose periodicity leads to a band structure analogous to the electronic band structure of semiconductors [8]. The implication of this analogy is the existence of photonic stopbands in which incident light of certain wavelengths is highly reflected due to its inability to propagate within the crystal [9]. By preferentially reflecting a narrow range of wavelengths, photonic crystals can reliably produce a characteristic color when illuminated with white light.

A more sophisticated approach involves gradually changing the period of the crystal. These “adiabatically chirped” photonic crystals (ACPCs) act as a locally periodic crystal for a range of wavelengths and can therefore reflect a broad swath of colors strongly, allowing for reflection spectra more complex than monochromatic color, e.g. the shiny shells of certain beetles [10–12] and eye glow of some butterflies [13–15]. The striking colors that can arise from ACPCs are shown in the case of gold and silver beetles in Fig. 1. An ACPC in the eye of a deep sea crustacean is shown in Fig. 2, where the chirped structure is signaled by gradual variations in the layer thickness.

Replication of natural photonic structures has already yielded marketable benefit in the manufacture of paints,

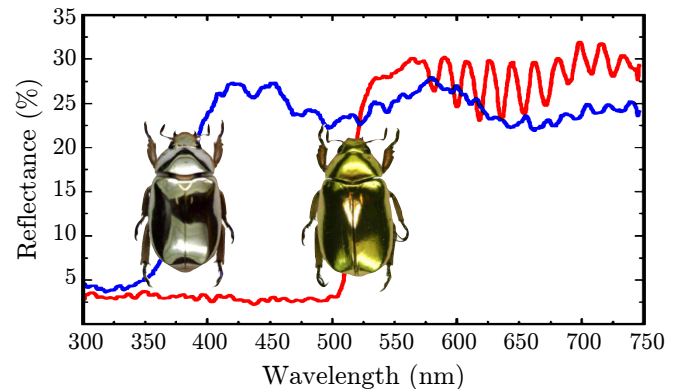


FIG. 1. *C. limbata* (left) and *C. aurigans* (right) displaying brilliant silver and gold color, respectively, due to reflection from ACPCs in their elytra. Figure adapted from Ref. [16].

fabrics, displays, and other technologies [5, 17]. ACPCs in particular are well-suited for applications requiring complex, broadband reflection spectra, such as light manipulation in white LEDs [17], dispersion control of ultrashort laser pulses [18], and tailored optical behavior in fiber gratings [19]. Better understanding the design of biological photonic structures such as ACPCs may therefore provide inspiration for future technologies.

There are many well-known tools for calculating the reflectance of dielectric multilayers, including transfer matrix methods and recursion techniques [2, 9, 21]. Although numerically exact, these methods are iterative, and when there are many layers involved, as in most biological applications, carrying out these computations does not solve the inverse problem of designing reflectors with tailored optical behavior. In this Letter, we instead derive an approximate, but closed-form, expression for the reflectance of ACPCs by matching Bloch wave expressions for the electric field across stopband regions via a *discrete* Wentzel-Kramers-Brillouin (WKB) method. Analysis of

* calebqcook@gmail.com

† arielamir@seas.harvard.edu

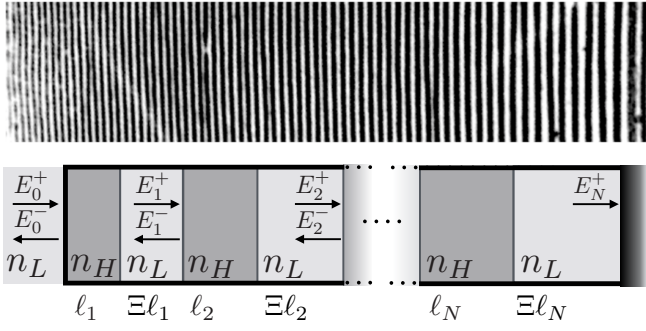


FIG. 2. *Top*: TEM image of an ACPC in the eye of the crustacean *C. refulgens*. Stained regions show layers, each on the order of 100 nm thick, of differing refractive index. Image taken from Ref. [20]. *Bottom*: Our model ACPC. Adiabatic chirp requires that the sequence of optical thicknesses ℓ_m varies slowly. The forward- and backward-propagating fields E_m^\pm are also shown, with an absorbing layer at the back enforcing $E_N^- = 0$.

this closed-form expression gives insight into several of the underlying the design principles of ACPCs.

Matuschek *et al.* [18] apply a related WKB approximation to study ACPCs for ultrafast laser application. However, their work makes several simplifying assumptions, such as ignoring reflections from the back of the multilayer and thereby assuming near perfect reflection.

$$F(x) = \frac{1}{1 - \rho^2} \begin{bmatrix} e^{i\pi x} - \rho^2 e^{-i\pi(\frac{1-\Xi}{1+\Xi})x} & -2i\rho e^{-i\pi(\frac{\Xi}{1+\Xi})x} \sin\left(\frac{\pi x}{1+\Xi}\right) \\ 2i\rho e^{i\pi(\frac{\Xi}{1+\Xi})x} \sin\left(\frac{\pi x}{1+\Xi}\right) & e^{-i\pi x} - \rho^2 e^{i\pi(\frac{1-\Xi}{1+\Xi})x} \end{bmatrix} \quad (2)$$

where $x = x_m(\lambda) = (1 + \Xi) \ell_m / (\lambda/2)$, and $\rho = (n_H - n_L) / (n_H + n_L)$ is the Fresnel reflection coefficient, which we assume to be small as is the case in nearly all biological ACPCs (see Table I).

When x is approximately integer, the transfer matrix recursion (1) has evanescent electric field solutions, corresponding to high reflectance of incident light. Wavelengths λ and bilayers m for which $x_m(\lambda)$ is approximately integer therefore define the *stopband* of the ACPC. Conversely, when x lies between integers Eq. (1) has oscillatory solutions, corresponding to low reflectance and hence defining the *passbands*. The bilayer indices $m_t(\lambda)$ which separate stopband/passband regions define the *turning points*. To avoid reflections between multiple stopbands and simplify our analysis, we assume just a single stopband $m \in [m_1(\lambda), m_2(\lambda)]$ for all considered wavelengths λ . We also assume an $x \approx 1$ stopband, since these require minimal layer thickness and are therefore most prevalent in biological systems.

In the case of no chirp $\ell_m = \ell$, the vector recursion (1)

By instead performing asymptotic matching in full, we obtain a reflectance expression that gives better agreement with numerically exact results. Our method also follows a more elementary approach and does not invoke a needlessly cumbersome coupled-mode formalism [22].

Consider a stack of $2N$ dielectric slabs of refractive indices $n_L < n_H$ arranged in an alternating fashion. We assume that within the m -th $\{n_L, n_H\}$ bilayer, the slabs have fixed optical thickness ratio $\Xi = (\ell_L)_m / (\ell_H)_m$. The sequence of optical thicknesses $\ell_m \equiv (\ell_H)_m = (\ell_L)_m / \Xi$ then encodes the chirp of the multilayer, which we assume to be monotonic and slowly-varying (compared to the wavelength of light) with bilayer index m . We also assume zero back-reflectance at the end of the ACPC, which models a final inhomogeneous absorptive layer, common to biological multilayers, whose light-diffusing character serves to strongly limit the amount of coherent radiation directed back into the structure [11, 12]. A depiction of the model is shown in Fig. 2.

In the transfer matrix method [21], one decomposes the electric field at each bilayer interface m into forward- and backward-propagating components $\mathbf{E}_m = \begin{bmatrix} E_m^+ \\ E_m^- \end{bmatrix}$. The fields \mathbf{E}_m at bilayer interfaces are related to one another via a transfer matrix product

$$\mathbf{E}_m = F_m(\lambda) \mathbf{E}_{m+1}. \quad (1)$$

For incident light of wavelength λ , the m -th bilayer transfer matrix $F_m(\lambda) = F(x)$ of our model is [23]

has exact, Bloch wave solutions $\mathbf{E}_m^\pm = \exp[-m \ln \mu^\pm] \mathbf{w}_m^\pm$ where $\mathbf{w}_m^\pm = \mathbf{w}^\pm$ are the transfer matrix eigenvectors with corresponding eigenvalues $\mu_m^\pm = \mu^\pm$. A natural generalization of these solutions are the modulated Bloch (mBloch) waves $\mathbf{E}_m^\pm = \exp[-\int^m \ln \mu_k^\pm dk] \mathbf{w}_m^\pm$, which approximately solve Eq. (1) for adiabatic chirp. Introducing the local Bloch phase $\varphi_m = \cos^{-1}[\text{Tr}(F_m)/2]$, approximate solutions to Eq. (1) are then given by linear combinations of mBloch waves

$$\mathbf{E}_m = C^+ \exp\left[i \int_m^{m_t} \varphi_k dk\right] \mathbf{w}_m^+ + C^- \exp\left[i \int_{m_t}^m \varphi_k dk\right] \mathbf{w}_m^- \quad (3)$$

with constant coefficients $C^\pm \in \{\{A, B\}, \{C, D\}, \{F, G\}\}$ in the three regions of the ACPC (passband \rightarrow stopband \rightarrow passband) separated by the turning points $m_{t=1,2}$.

Higher order corrections to the mBloch wave solution (3) are obtained in Section I of the Supplementary Material by demanding local energy conservation in the multilayer. These corrections diverge at turning points $m_{1,2}$, which we overcome by studying Eq. (1) in more detail near these

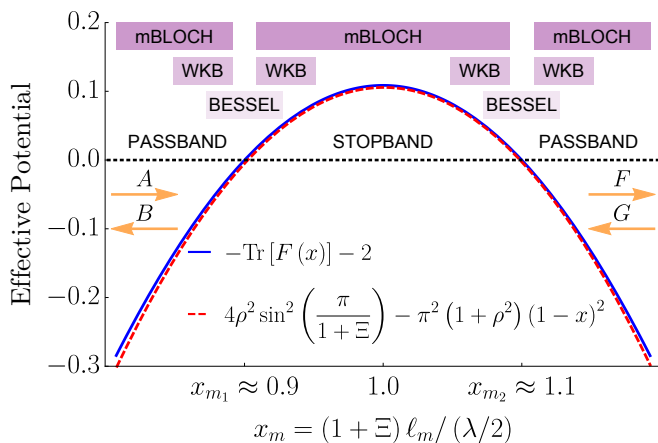


FIG. 3. Plot of the stopband potential $-\text{Tr}[F(x)] - 2$ and its quadratic expansion about $x = \Xi = 1$ and $\rho = 0$ in the quantum scattering analogy (detailed in Section II of the Supplementary Material) for an ACPC with $n_L = 1.0$, $n_H = 1.4$, and $\Xi = 0.75$. The regions of validity for various approximate expressions for E_m^\pm are sketched. The WKB matching formulae (derived in Section III of the Supplementary Material) relate the pre-stopband coefficients A , B and the post-stopband coefficients F , G in the mBloch wave solution (3).

points. In particular, adiabatic chirp implies that near a given bilayer m , the fields E_m^\pm approximately satisfy the recurrence

$$E_{m+1}^\pm \approx \text{Tr}(F_m)E_m^\pm - E_{m-1}^\pm \quad (4)$$

which is formally a discrete Schrödinger equation in a potential determined by $\text{Tr}(F_m)$ (see Section II of the Supplementary Material for details). We therefore apply a discrete WKB method [25, 26] to approximately solve Eq. (4) near the turning points $m_{1,2}$ and match the mBloch wave (3) coefficients \mathcal{C}^\pm across the ACPC stopband. We sketch this procedure in Fig. 3.

The ratio of fields E_0^-/E_0^+ in the mBloch solution (3) is fixed by enforcing the absorber condition $E_N^- = 0$ and applying the discrete WKB matching formulae, which are characterized by the tunneling exponent

$$\begin{aligned} \gamma(\lambda) &= \int_{m_1(\lambda)}^{m_2(\lambda)} \cosh^{-1} \left\{ -\frac{\text{Tr}[F_m(\lambda)]}{2} \right\} dm \\ &\approx \frac{\lambda}{q(\lambda)} \sin^2 \left(\frac{\pi}{1+\Xi} \right) \rho^2 + \mathcal{O}(\rho^3) \end{aligned} \quad (5)$$

where $q(\lambda) \equiv (1+\Xi) \frac{d\ell}{dm}$ ($\ell = \frac{\lambda/2}{1+\Xi}$) is the chirp rate at the center of stopband. In approximating Eq. (5), we have used the quadratic expansion of $\text{Tr}(F_m)$ shown in Fig. 3. The reflectance $R = |E_0^-/E_0^+|^2$ of ACPCs calculated via this discrete WKB matching procedure is then given to lowest order in ρ by

$$\tilde{R}(\lambda) = 1 - \exp[-2\gamma(\lambda)], \quad (6)$$

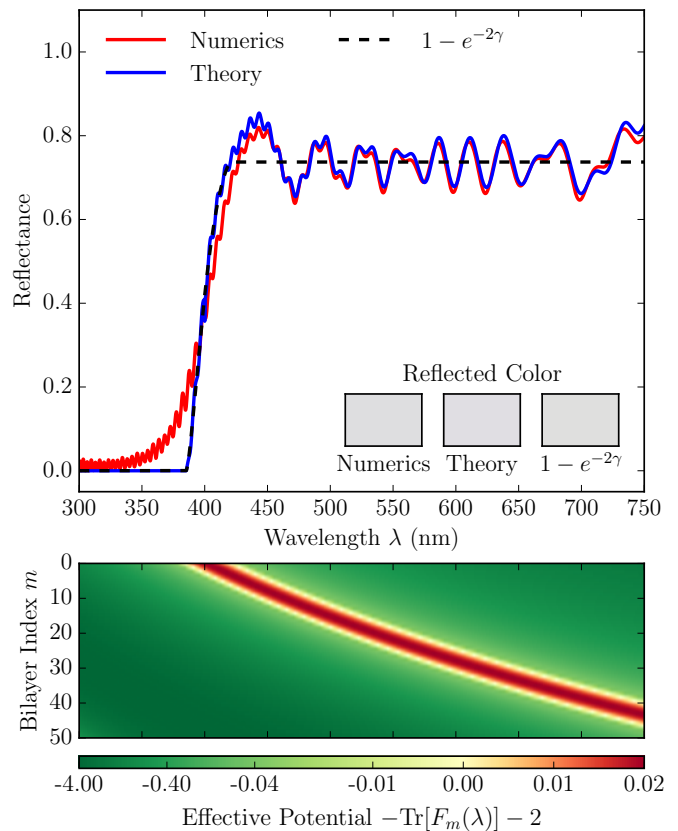


FIG. 4. An exponentially chirped photonic crystal with $n_L = 1.34$, $n_H = 1.54$, and $\Xi = 1$. *Top*: A comparison between the numerically exact transfer matrix (red), first-order WKB (Eq. (S18), blue), and zeroth-order WKB (Eq. (6), dashed) reflection spectra is shown. *Bottom*: The analogous quantum potential of the ACPC is plotted for each incident wavelength.

analogous to the form found in quantum scattering [27]. This calculation is detailed in Section I of the Supplementary Material, where the next-order WKB reflectance is also given in Eq. (S18). A comparison between the numerically exact reflection spectrum of an ACPC and our corresponding WKB results (6) and (S18) is shown in Fig. 4. As Fig. 4 demonstrates, the WKB expression $\tilde{R}(\lambda)$ (6) in fact captures a moving average of the exact reflectance spectrum.

Dimensional analysis shows that $q(\lambda)$ in Eq. (5), when written in terms of the wavelengths $\lambda_{\min} = 2(1+\Xi)\ell_0$ and $\lambda_{\max} = 2(1+\Xi)\ell_N$ over which an ACPC reflects strongly, is independent of the optical thickness ratio Ξ . The tunneling exponent $\gamma(\lambda)$ (5) and hence the average reflectance $\tilde{R}(\lambda)$ (6) is therefore maximal for $\Xi = 1$, i.e. when the optical thicknesses are equal in each bilayer. For periodic $\ell_m = \ell$ reflectors, the above fact is well-known, and such multilayers have been dubbed "ideal" [4]. Our results therefore generalize the claim that ideal bilayers elicit maximal reflectance to the case of periodicity-breaking adiabatic chirp.

Our results can also be used to solve the following design

| Adiabatically Chirped Photonic Crystal | n_L | n_H | Ξ | λ_{\min} | λ_{\max} | N | $N_{\text{exp}}^{\gamma \sim 1}$ | $N_{\text{lin}}^{\gamma \sim 1}$ | Ref. |
|--|-------|-------|-------|------------------|------------------|-----------|----------------------------------|----------------------------------|------|
| <i>Aspidomorpha tecta</i> (beetle) elytra | 1.40 | 1.68 | 0.79 | 450 | 850 | ~ 44 | 40 (-9%) | 56 (+27%) | [11] |
| <i>Chrysin aurigans</i> (beetle) elytra | 1.57 | 1.80 | 1.10 | 520 | 1000 | ~ 94 | 71 (-24%) | 100 (+6%) | [28] |
| <i>Cephalophanes refulgens</i> (crustacean) eyes | 1.34 | 1.54 | 0.87 | 350 | 700 | ~ 75 | 73 (-3%) | 105 (+40%) | [20] |
| <i>Danaella</i> sp. (crustacean) antennae | 1.34 | 1.54 | 0.86 | 370 | 700 | ~ 74 | 67 (-9%) | 94 (+27%) | [29] |
| <i>Danaus plexippus</i> (butterfly) tapeta | 1.00 | 1.40 | 0.63 | 300 | 550 | ~ 44 | 12 (-73%) | 17 (-61%) | [15] |
| <i>Vanessa cardui</i> (butterfly) tapeta | 1.00 | 1.50 | 0.64 | 320 | 680 | ~ 35 | 11 (-63%) | 16 (-54%) | [30] |

TABLE I. Comparison between the number of bilayers N found in several biological ACPCs and our predicted minimal number $N_{\text{exp/lin}}^{\gamma \sim 1}$ (8). The percent difference between N and $N_{\text{exp/lin}}^{\gamma \sim 1}$ is given in the relevant column. All wavelengths $\lambda_{\min, \max}$ given in nanometers. The optical thickness ratio Ξ in each case is estimated via analysis of TEM images given in the corresponding reference (see Section IV of the Supplementary Material).

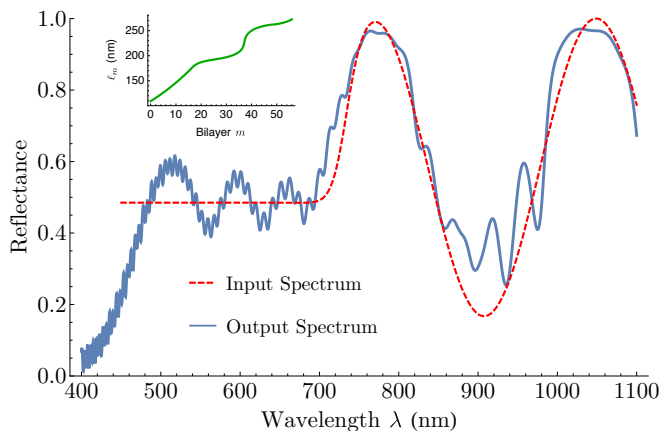


FIG. 5. An ACPC with a designed average reflectance spectrum. The desired spectrum (red) is put into the chirp differential equation (7) with $n_H = 1.54$ and $n_L = 1.34$, which is solved numerically to give the chirp function ℓ_m plotted in the inset (green). The resulting exact reflectance (blue) of the computed chirp ℓ_m is then found numerically via transfer matrices and plotted against the input spectrum.

problem: given a desired average reflectance spectrum $\tilde{R}(\lambda)$, what chirp function ℓ_m is required to elicit $\tilde{R}(\lambda)$? Solving Eqs. (5) and (6) for $d\ell/dm$ reveals that this question can be answered by simply solving the differential equation

$$\frac{d\ell}{dm} = \frac{-4\rho^2 \sin^2\left(\frac{\pi}{1+\Xi}\right)}{\log\left[1 - \tilde{R}\left(\lambda = 2(1+\Xi)\ell\right)\right]} \ell. \quad (7)$$

The chirp differential equation (7) offers a novel method of designing multilayer reflectors of tailored optical behavior, and we exhibit such a design spectrum in 5. Moreover, Eq. (7) shows that achieving a flat spectrum $\tilde{R}(\lambda) = \tilde{R}$ requires exponential chirp of the form $\ell_m = \ell_0 (\ell_N/\ell_0)^{m/N}$. Constant reflectance and hence exponential chirp are of special interest since reflectance above some threshold value is minimally achieved with a flat spectrum.

By computing $q(\lambda)$ in Eq. (5) for specified chirp functions, we can in fact calculate the minimal number of bilayers N required to exceed some reflectance \tilde{R} over a

given range of wavelengths. For comparison, we carry out this calculation for both exponential $\ell_m = \ell_0 (\ell_N/\ell_0)^{m/N}$ and linear $\ell_m = \ell_0 + (\ell_N - \ell_0)(m/N)$ chirps, which gives the minimal bilayer numbers

$$N = \frac{\log\left(\frac{1}{1-\tilde{R}}\right)}{4\rho^2 \sin^2\left(\frac{\pi}{1+\Xi}\right)} \times \begin{cases} \log(\lambda_{\max}/\lambda_{\min}), & \text{(exponential)} \\ \lambda_{\max}/\lambda_{\min} - 1, & \text{(linear)} \end{cases} \quad (8)$$

Note that (i) Eq. (8) is minimized in either case for $\Xi = 1$ and (ii) $N_{\text{exp}} \leq N_{\text{lin}}$, consistent with our earlier conclusions. We also emphasize that the design principles contained in Eqs. (7) and (8) are not inferable via traditional, numerical (e.g. transfer matrix) approaches.

Comparison between the number of bilayers N found in several biological ACPCs and our predicted minimal number $N_{\text{exp/lin}}$ (8) gives a quantitative measure of the optimality of ACPCs in nature. In order to make a concrete comparison, we fix an arbitrary high reflectance benchmark of $\gamma \sim 1$, i.e. $\tilde{R} \sim 86\%$. This comparison is shown in Table I for several ACPCs in nature and reveals that biological ACPCs are generally less optimal than exponentially chirped reflectors but generally more optimal than their linearly chirped counterparts.

Exceptions to the above conclusion are the butterfly tapeta highlighted in Table I, which have many more bilayers than expected per our analysis. This is consistent, however, with the fact that optical components such as tapeta likely require near perfect reflection, corresponding to $\gamma > 1$ and a greater number of bilayers in Eq. (8). Indeed, this explanation is supported by the fact that the reported reflection spectra of *D. plexippus* [15] and *V. cardui* [30] tapeta are essentially unity $\tilde{R} \approx 1$ over the range of wavelengths $[\lambda_{\min}, \lambda_{\max}]$.

In summary, our closed-form results allow for tailoring ACPCs of desired reflectance spectra and estimating the optimality of chirped reflectors in nature. More generally, the mathematical methods developed herein are applicable to coupled wave propagation in slowly-varying media and therefore also relevant to the design of mechanical and acoustic metamaterials.

We thank Dvir Gur, Pete Vukusic, Gary Bernard, and Mark Arildsen for helpful discussions. C.Q.C. acknowledges support from the Harvard College Research Pro-

gram and the Perimeter Institute. Research at PI is supported by the Government of Canada through Indus-

try Canada and by the Province of Ontario through the Ministry of Research and Innovation. A.A. thanks the support of the Alfred P. Sloan Foundation.

-
- [1] S. Johnsen, *The Optics of Life: A Biologist's Guide to Light in Nature* (Princeton University Press, 2012).
- [2] S. Kinoshita, *Structural Colors in the Realm of Nature* (World Scientific, 2008).
- [3] S. Kinoshita, S. Yoshioka, and J. Miyazaki, *Reports on Progress in Physics* **71**, 076401 (2008).
- [4] M. F. Land, *Progress in Biophysics and Molecular Biology* **24**, 75 (1972).
- [5] P. Vukusic and J. R. Sambles, *Nature* **424**, 852 (2003).
- [6] G. S. Smith, *American Journal of Physics* **77**, 1010 (2009).
- [7] L. Biró and J. Vigneron, *Laser & Photonics Reviews* **5**, 27 (2011).
- [8] J. D. Joannopoulos, S. G. Johnson, J. N. Winn, and R. D. Meade, *Photonic Crystals: Molding the Flow of Light* (Princeton University Press, 2011).
- [9] A. Amir and P. Vukusic, *American Journal of Physics* **81**, 253 (2013).
- [10] A. C. Neville, *Journal of Insect Physiology* **23**, 1267 (1977).
- [11] A. R. Parker, D. R. McKenzie, and M. C. Large, *The Journal of Experimental Biology* **201**, 1307 (1998).
- [12] D. Azofeifa, M. Hernández-Jiménez, E. Libby, A. Solís, C. Barboza-Aguilar, and W. Vargas, *Journal of Quantitative Spectroscopy and Radiative Transfer* **160**, 63 (2015).
- [13] W. H. Miller and G. D. Bernard, *Journal of Ultrastructure Research* **24**, 286 (1968).
- [14] W. A. Ribi, *Endeavour* **5**, 2 (1981).
- [15] T. Labhart, F. Baumann, and G. D. Bernard, *Cell and Tissue Research* **338**, 391 (2009).
- [16] C. Campos-Fernández, D. E. Azofeifa, M. Hernández-Jiménez, A. Ruiz-Ruiz, and W. E. Vargas, *Opt. Mater. Express* **1**, 85 (2011).
- [17] K. Yu, T. Fan, S. Lou, and D. Zhang, *Progress in Materials Science* **58**, 825 (2013).
- [18] N. Matuschek, F. X. Kartner, and U. Keller, *IEEE Journal of Selected Topics in Quantum Electronics* **4**, 197 (1998).
- [19] T. Erdogan, *Journal of Lightwave Technology* **15**, 1277 (1997).
- [20] S. Nishida, S. Ohtsuka, and A. R. Parker, *Marine Ecology Progress Series* **227**, 157 (2002).
- [21] F. Abelés, *Ann. Phys. (Paris)* **5**, 596 (1950).
- [22] N. Matuschek, F. X. Kartner, and U. Keller, *IEEE Journal of Quantum Electronics* **33**, 295 (1997).
- [23] S. J. Orfanidis, *Electromagnetic Waves and Antennas* (Rutgers University New Brunswick, NJ, 2002).
- [24] See Supplemental Material for details.
- [25] R. B. Dingle and G. J. Morgan, *Applied Scientific Research* **18**, 221 (1968).
- [26] P. A. Braun, *Rev. Mod. Phys.* **65**, 115 (1993).
- [27] E. Merzbacher, *Quantum Mechanics*, 3rd ed. (Wiley, New York, 1998).
- [28] E. Libby, D. E. Azofeifa, M. Hernández-Jiménez, C. Barboza-Aguilar, A. Solís, I. Garca-Aguilar, L. Arce-Marengo, A. Hernández, and W. E. Vargas, *Journal of Optics* **16**, 082001 (2014).
- [29] A. R. Parker, in *Crustaceans and the biodiversity crisis (Crustaceana)* (1999) pp. 879–887.
- [30] A. D. Briscoe, G. D. Bernard, A. S. Szeto, L. M. Nagy, and R. H. White, *The Journal of Comparative Neurology* **458**, 334 (2003).
- [31] A. Garg, *Journal of Mathematical Physics* **39**, 5166 (1998).
- [32] H. Bremmer, *Physica* **15**, 593 (1949).
- [33] M. V. Berry and K. E. Mount, *Reports on Progress in Physics* **35**, 315 (1972).
- [34] P. A. Braun, *Theoretical and Mathematical Physics* **37**, 1070 (1978).
- [35] P. Wilmott, *IMA Journal of Applied Mathematics* **34**, 295 (1985).
- [36] J. S. Geronimo and D. T. Smith, *Journal of Approximation Theory* **69**, 269 (1992).
- [37] A. Garg, *Phys. Rev. Lett.* **83**, 4385 (1999).
- [38] N. W. Ashcroft and N. D. Mermin, *Solid State Physics* (Saunders College, 1976).
- [39] M. Abramowitz and I. A. Stegun, *Handbook of Mathematical Functions with Formulas, Graphs, and Mathematical Tables* (Dover, 1964) tenth printing, with corrections (December 1972).

Theory of chirped photonic crystals in biological broadband reflectors: *Supplementary Material*

I. DERIVATION OF WKB REFLECTANCE

In this section, we outline the calculation of the WKB expression for the reflectance of adiabatic chirped photonic crystals presented in the main text. We also give the WKB reflectance calculated to the next order in ρ .

As presented in the main text, the wavelength-dependent bilayer transfer matrix $F_m(\lambda)$, relating the forward- and backward-propagating electric fields

$$\mathbf{E}_m = \begin{bmatrix} E_m^+ \\ E_m^- \end{bmatrix} \quad (\text{S1})$$

via the vector recursion relation

$$\mathbf{E}_m = F_m(\lambda) \mathbf{E}_{m+1}, \quad (\text{S2})$$

for our model takes the form

$$F_m(\lambda) = \begin{bmatrix} X_m(\lambda) & Y_m(\lambda) \\ Y_m^*(\lambda) & X_m^*(\lambda) \end{bmatrix} \quad (\text{S3})$$

with complex matrix elements $X_m(\lambda)$, $Y_m(\lambda)$ satisfying $\det F_m(\lambda) = |X_m|^2 - |Y_m|^2 = 1$. The eigenvectors \mathbf{w}_m^\pm and corresponding eigenvalues μ_m^\pm of the general transfer matrix F_m are explicitly

$$\mathbf{w}_m^\pm = D_m^\pm \begin{bmatrix} 1 \\ \left(\frac{\mu_m^\pm - X_m}{Y_m} \right) \end{bmatrix} \quad (\text{S4})$$

and

$$\mu_m^\pm = \left(\frac{X_m + X_m^*}{2} \right) \pm \sqrt{\left(\frac{X_m + X_m^*}{2} \right)^2 - 1}, \quad (\text{S5})$$

where the D_m^\pm are eigenvector normalizations, which we will discuss in more detail shortly.

In the main text it is shown that linear combinations of modulated Bloch waves

$$\mathbf{E}_m = \sum_{i=\pm} C^i \exp \left[- \int^m \ln \mu_k^i dk \right] \mathbf{w}_m^i \quad (\text{S6})$$

approximately solve the transfer matrix recursion (S2) in the limit of adiabatic chirp. One could proceed by seeking higher-order corrections to the modulated Bloch wave solution (S6), but we instead invoke energy conservation to find the m -dependence of the eigenvector normalizations D_m^\pm and thereby extract the dominant effect of these corrections [31]. From Eqs. (S5) and (S6) we calculate the Poynting energy flux density $\mathcal{P}_m \propto |E_m^+|^2 - |E_m^-|^2$ [23] to be

$$\mathcal{P}_m \propto \begin{cases} |C^+|^2 |D_m^+|^2 \left(\frac{\mu_m^+ - \mu_m^-}{\mu_m^+ - X_m^*} \right) - |C^-|^2 |D_m^-|^2 \left(\frac{\mu_m^+ - \mu_m^-}{\mu_m^- - X_m^*} \right) & (\text{passband}) \\ (C^+ D_m^+) (B D_m^-)^* \left(\frac{\mu_m^+ - \mu_m^-}{\mu_m^+ - X_m^*} \right) - (C^+ D_m^+)^* (C^- D_m^-) \left(\frac{\mu_m^+ - \mu_m^-}{\mu_m^- - X_m^*} \right) & (\text{stopband}) \end{cases} \quad (\text{S7})$$

which *a priori* depends on the bilayer index m . However, taking the eigenvector normalizations D_m^\pm to scale as

$$D_m^\pm \sim \sqrt{\frac{\mu_m^\pm - X_m^*}{\mu_m^\pm - \mu_m^\mp}}. \quad (\text{S8})$$

removes the m -dependence of $\mathcal{P}_m = \mathcal{P}$ (S7) and therefore enforces constant energy flux density in the multilayer, as required by energy conservation. The modulated Bloch wave solution (S6) with the eigenvector normalizations (S8) is a generalization of the Bremmer method for deriv-

ing WKB-type solutions [32, 33].

As a turning point $m \rightarrow m_{1,2}$ in the multilayer is approached, the transfer matrix eigenvalues (S5) $\mu_m^+ \rightarrow \mu_m^-$ converge to one another and the required eigenvector normalizations D_m^\pm (S8) become arbitrarily large. This implies that our assumption of slowly varying transfer matrix eigenvectors \mathbf{w}_m^\pm breaks down and our approximate solution (S6) no longer holds near the turning points $m \sim m_{1,2}$, even in the case of adiabatic chirp. We must therefore write general solutions of the form (S6) separately in the three regions of the multilayer separated by the turning points m_1 and m_2 , giving

$$\begin{bmatrix} E_m^+ \\ E_m^- \end{bmatrix} = \begin{cases} A \exp \left\{ i \int_m^{m_1} \cos^{-1} \left(\frac{a_k}{2} \right) dk \right\} \mathbf{w}_m^+ + B \exp \left\{ -i \int_m^{m_1} \cos^{-1} \left(\frac{a_k}{2} \right) dk \right\} \mathbf{w}_m^- & (m < m_1) \\ (-1)^m \left[C \exp \left\{ \int_{m_1}^m \cosh^{-1} \left(-\frac{a_k}{2} \right) dk \right\} \mathbf{w}_m^- + D \exp \left\{ -\int_{m_1}^m \cosh^{-1} \left(-\frac{a_k}{2} \right) dk \right\} \mathbf{w}_m^+ \right] & (m_1 < m < m_2) \\ F \exp \left\{ -i \int_{m_2}^m \cos^{-1} \left(\frac{a_k}{2} \right) dk \right\} \mathbf{w}_m^+ + G \exp \left\{ i \int_{m_2}^m \cos^{-1} \left(\frac{a_k}{2} \right) dk \right\} \mathbf{w}_m^- & (m_2 < m) \end{cases} \quad (\text{S9})$$

where we have introduced the complex coefficients A , B , C , D , F , and G , in addition to the trace $a_m(\lambda) \equiv \text{Tr}[F_m(\lambda)]$ whose magnitude determines the complex structure of the transfer matrix eigenvalues μ_m^\pm , so that

$$\begin{cases} |a_m(\lambda)| < 2 \iff m \in \text{passband} \\ |a_m(\lambda)| > 2 \iff m \in \text{stopband} \\ |a_m(\lambda)| = 2 \iff m \text{ is a turning point} \end{cases} \quad (\text{S10})$$

Since our modulated Bloch wave solution (S9) breaks down near turning points $m \sim m_{1,2}$, we return to the exact vector recurrence (S2), which may be approximated in the limit of adiabatic chirp as

$$\mathbf{E}_{m+1} + \mathbf{E}_{m-1} = (F_m^{-1} + F_{m-1}) \mathbf{E}_m \approx a_m \mathbf{E}_m \quad (\text{S11})$$

in the vicinity of a given bilayer m . This implies that we can treat E_m^\pm as decoupled fields each independently satisfying the recurrence relation

$$E_{m+1}^\pm = a_m E_m^\pm - E_{m-1}^\pm \quad (\text{S12})$$

near turning points $m \sim m_{1,2}$. A discrete form of the Wentzel-Kramers-Brillouin (WKB) method [25, 26, 34–36] then allows us to approximately solve Eq. (S12) in the vicinity of turning points $m \sim m_{1,2}$ and match the modulated Bloch waves (S9) across the stopband region $m \in [m_1, m_2]$.

The discrete WKB method has traditionally found application in approximate calculations of quantum mechanical energy spectra [26, 31, 34, 37]. The discrete WKB method in the present context is detailed in Section III, with discrete WKB solutions to the difference equation (S12) given by Eq. (S36).

Crucially, the discrete WKB solutions (S36) share the same functional form as the modulated Bloch waves (S9) in the vicinity of a turning point $m \sim m_{1,2}$, since in that limit the transfer matrix eigenvector normalizations (S8) become

$$D_m^+ \sim D_m^- \sim (\mu_m^+ - \mu_m^-)^{-1/2} = (a_m^2 - 4)^{-1/4} \quad (\text{S13})$$

and Eq. (S9) subsequently reduces to the discrete WKB solutions (S36). We therefore identify the complex coefficients A, \dots, G in the modulated Bloch wave solution (S9) with the analogous coefficients in the discrete WKB solution (S36). Applying an asymptotic matching procedure to the discrete WKB solution coefficients, and hence the modulated Bloch wave coefficients A, B, F , and G , then allows for patching of the modulated Bloch waves (S9) across the stopband region.

Asymptotic matching of the discrete WKB solutions is performed in Section III, and the resulting connection formulae across an $x_m \approx 1$ (or more generally, $a_m < -2$) stopband $m \in [m_1, m_2]$ are given by

$$\begin{bmatrix} A \\ B \end{bmatrix} = \begin{bmatrix} \alpha & \beta \\ \beta^* & \alpha^* \end{bmatrix} \begin{bmatrix} F \\ G \end{bmatrix} \quad (\text{S14})$$

where we have introduced the variables

$$\alpha(\lambda) = e^{i[m_2(\lambda) - m_1(\lambda)]\pi} \left[e^{\gamma(\lambda)} + \frac{1}{4} e^{-\gamma(\lambda)} \right] \quad (\text{S15})$$

$$\beta(\lambda) = -i e^{-i[m_2(\lambda) + m_1(\lambda)]\pi} \left[e^{\gamma(\lambda)} - \frac{1}{4} e^{-\gamma(\lambda)} \right] \quad (\text{S16})$$

$$\gamma(\lambda) = \int_{m_1(\lambda)}^{m_2(\lambda)} \cosh^{-1} \left[-\frac{a_m(\lambda)}{2} \right] dm \quad (\text{S17})$$

The parameter γ is analogous to the tunneling exponent in the Gamow theory of alpha decay [27], in which the probability T of He^{2+} emission from an atomic nucleus satisfies $T \sim e^{-2\gamma}$. In the present case, $\gamma(\lambda)$ (S17) characterizes how deeply light of wavelength λ penetrates an $a_m < -2$ stopband of a chirped photonic crystal.

The terminating absorber condition $E_N^- = 0$ assumed in our model gives a linear relation between the coefficients F and G in the modulated Bloch wave solution (S9) and thus a linear relation between the coefficients A and B via the discrete WKB matching formulae (S14). This linear relation fixes A/B and hence the field ratio $r = E_0^-/E_0^+$ through the modulated Bloch wave solution (S9). The reflectance $R = |r|^2$ of ACPCs calculated in this way is given by

$$R(\lambda) = \tilde{R}(\lambda) + 2\rho\sqrt{\tilde{R}(\lambda)} \left[1 - \tilde{R}(\lambda) \right] \left\{ \frac{\sin(2\pi\ell_0/\lambda)}{\sin[2\pi(1+\Xi)\ell_0/\lambda]} \sin 2\phi_0 - \frac{\sin(2\pi\ell_N/\lambda)}{\sin[2\pi(1+\Xi)\ell_N/\lambda]} \sin 2\phi_N \right\} + \mathcal{O}(\rho^2) \quad (\text{S18})$$

where we have again introduced the zeroth-order WKB

reflectance

$$\tilde{R}(\lambda) = 1 - \exp[-2\gamma(\lambda)]. \quad (\text{S19})$$

as well as the phase angles

$$\phi_0(\lambda) = \int_0^{m_1(\lambda)} \cos^{-1} \left[\frac{a_m(\lambda)}{2} \right] dm - m_1(\lambda) \pi \quad (\text{S20})$$

$$\phi_N(\lambda) = \int_{m_2(\lambda)}^N \cos^{-1} \left[\frac{a_m(\lambda)}{2} \right] dm + m_2(\lambda) \pi \quad (\text{S21})$$

II. TIGHT-BINDING ANALOGY

In this section, we make an analogy between the electric fields E_m^\pm in an adiabatically chirped photonic crystal and the zero energy eigenmodes of a one-dimensional chain, described quantum mechanically by a tight-binding Hamiltonian. Naively applying the continuous WKB method to the quantum chain yields results consistent with those of the discrete WKB analysis near turning points and offers insight into the functional form of E_m^\pm and our matching formulae. By taking a continuum limit of the quantum chain tight-binding Hamiltonian, we also make concrete the analogy between the reflection of light from a photonic stopband and quantum scattering from a potential barrier.

We note that the recurrence relation (S12) is precisely the equation one would obtain by seeking the zero energy eigenmodes E_m of a Hamiltonian H given by

$$H = \begin{bmatrix} a_1 & -1 & & & \\ -1 & a_2 & \ddots & & \\ & -1 & \ddots & -1 & \\ & & \ddots & a_{N-1} & -1 \\ & & & -1 & a_N \end{bmatrix}. \quad (\text{S22})$$

We can view the matrix H as a tight-binding Hamiltonian of a finite, one-dimensional quantum chain with nearest-neighbor hopping elements [38].

Let us first begin with the simple case that $a_m = a$ is constant. In this case, we can write the exact eigenmode solution as a discrete plane wave $E_m = e^{\pm i\kappa m}$ with wavevector κ . Substitution into our recurrence relation (S12) then tells us that

$$e^{i\kappa} + e^{-i\kappa} = a \quad (\text{S23})$$

which implies that our wavevector κ is given by

$$\kappa = \begin{cases} \cos^{-1}(a/2), & a \in [-2, 2] \\ i \cosh^{-1}(a/2), & a > 2 \\ i \cosh^{-1}(a/2) + \pi, & a < -2 \end{cases}. \quad (\text{S24})$$

The general eigenmode solution E_m in the constant $a_m = a$ case is then just a linear superposition

$$E_m = Ae^{i\kappa m} + Be^{-i\kappa m} \quad (\text{S25})$$

of the discrete plane waves of wavevectors $\pm\kappa$. When $a \in [-2, 2]$ and κ is real, the zero energy eigenmode

components E_m are oscillatory in the bilayer/chain site index m . Conversely, when $|a| > 2$ and κ is imaginary, the components E_m are the sum of growing and decaying exponentials in the index m .

In the more general case that a_m varies slowly with bilayer/chain site index m , we can write the continuous WKB solution to the above eigenmode problem as [27]

$$E_m \propto \frac{1}{\sqrt{\kappa_m}} e^{\pm i \int^m \kappa_k dk}. \quad (\text{S26})$$

Substituting this expression into our recursion relation gives, to lowest order in the variation of κ_m with respect to m , the same consistency equation as before

$$e^{i\kappa_m} + e^{-i\kappa_m} = a_m \quad (\text{S27})$$

which implies (variable) wavevector solutions

$$\kappa_m = \begin{cases} \cos^{-1}(a_m/2), & a_m \in [-2, 2] \\ i \cosh^{-1}(a_m/2), & a_m > 2 \\ i \cosh^{-1}(a_m/2) + \pi, & a_m < -2 \end{cases}. \quad (\text{S28})$$

Again, the magnitude of a_m tells us whether the the eigenmode components E_m are oscillatory or exponential in the index m .

Comparing the continuum WKB result (S26) with the form of E_m obtained via the discrete WKB method (S36), we see that the two differ only by the m -dependence of the passband magnitude $|E_m|$ of the electric field/zero energy eigenmode. In particular,

$$|E_m| = \begin{cases} [\cos^{-1}(a_m/2)]^{-1/2} & (\text{S26}) \\ (4 - a_m^2)^{-1/4} & (\text{S36}) \end{cases} \quad (\text{S29})$$

in passband regions $|a_m| < 2$. However, these two forms are consistent to lowest order in $(a_m \pm 2)$, i.e. near turning points, which is precisely the regime in which the difference equation (S12) is applied in Section III to match the modulated Bloch waves (S9). This explains the strong similarity (exact agreement) between the standard WKB connection formulae [27] and the discrete WKB matching formulae across an odd (even) stopband and given in Section III.

We can gain further intuition from this tight-binding analogy by rewriting the tight-binding Hamiltonian H in the continuum limit as

$$H \rightarrow -\frac{d^2}{dz^2} + [a(z) - 2] = \left(-i \frac{d}{dz}\right)^2 + V(z) \quad (\text{S30})$$

where $m \rightarrow z$ represents the continuous coordinate parametrizing the depth in the multilayer and/or length along the quantum chain, and we have introduced the potential

$$V(z) = a(z) - 2. \quad (\text{S31})$$

Examining the continuum quantum chain potential $V(z)$ reveals why one obtains evanescent solutions when

$a(z) > 2$; in this case the potential (S31) is positive, and therefore the zero energy modes we seek are classically forbidden by energy conservation. In quantum mechanics, however, such classically forbidden solutions to $HE(z) = 0$ are allowed, but are exponentially damped in z due to quantum tunneling [27].

An identical analogy can be made for odd $a(z) < -2$ stopbands by transforming the recurrence (S12) in E_m to the recurrence

$$-\tilde{E}_{m+1} + \tilde{a}_m \tilde{E}_m - \tilde{E}_{m-1} = 0 \quad (\text{S32})$$

III. DERIVATION OF DISCRETE WKB CONNECTION FORMULAE

In this section, we first derive the discrete WKB connection formulae across an even, i.e. $a_m > 2$, stopband and then apply a transformation to the recurrence (S12) to obtain the analogous connection formulae across an odd, $a_m < -2$, stopband. These results connect *scattering* states E_m^\pm across a classically forbidden region and augment the discrete WKB matching procedure used by Braun [34] to derive the quantization rules for *bound* states.

Since both E_m^+ and E_m^- (approximately) satisfy the same recursion relation

$$E_{m+1}^\pm = a_m E_m^\pm - E_{m-1}^\pm \quad (\text{S34})$$

near a turning point $m \sim m_{1,2}$, it suffices to consider just E_m^+ . Approximate discrete WKB expressions for the field E_m^+ can be obtained by assuming a solution to the above recurrence relation of the form

$$E_m^+ = \exp \left\{ i \left[\Phi_m^0 + \Phi_m^1 + \Phi_m^2 + \dots \right] \right\} \quad (\text{S35})$$

where the unknown functions Φ_m^j are labeled according to their rate of change with respect to the index m , so that $\dot{\Phi}_m^j = \mathcal{O}(m^{-j})$, $\ddot{\Phi}_m^j = \mathcal{O}(m^{-j-1})$, and so on. Substituting the discrete WKB ansatz (S35) into the recurrence relation (S34) and solving for the unknown functions Φ_m^j up to order $\mathcal{O}(m^{-1})$ yields [26, 34]:

$$E_m^+ = \begin{cases} \frac{1}{\sqrt[4]{4 - a_m^2}} \left[A \exp \left\{ i \int_{m_1}^m \cos^{-1} \left(\frac{a_k}{2} \right) dk \right\} + B \exp \left\{ -i \int_{m_1}^m \cos^{-1} \left(\frac{a_k}{2} \right) dk \right\} \right] & (m < m_1) \\ \frac{1}{\sqrt[4]{a_m^2 - 4}} \left[C \exp \left\{ \int_{m_1}^m \cosh^{-1} \left(\frac{a_k}{2} \right) dk \right\} + D \exp \left\{ - \int_{m_1}^m \cosh^{-1} \left(\frac{a_k}{2} \right) dk \right\} \right] & (m_1 < m < m_2) \\ \frac{1}{\sqrt[4]{4 - a_m^2}} \left[F \exp \left\{ -i \int_{m_2}^m \cos^{-1} \left(\frac{a_k}{2} \right) dk \right\} + G \exp \left\{ i \int_{m_2}^m \cos^{-1} \left(\frac{a_k}{2} \right) dk \right\} \right] & (m_2 < m) \end{cases} \quad (\text{S36})$$

Our goal is to match these solutions across the stopband, i.e. find a linear relationship between the coefficients A , B and F , G . Performing this matching procedure will require analysis of approximate solutions to original recurrence (S12) in the vicinity of each turning point, which we obtain by linearizing a_m near m_1 and m_2 .

A. Even Stopband Connection Formulae

Suppose we have an $a_m > 2$ stopband for $m \in [m_1, m_2]$ (where m_1, m_2 are not necessarily integers), surrounded on either side by propagation bands $|a_m| < 2$.

1. Matching Across Even $m = m_1$ Turning Point

When linearized near m_1 , the recurrence (S12) takes the form

$$E_{m+1}^+ = [2 + \alpha_1 (m - m_1)] E_m^+ - E_{m-1}^+ \quad (\text{for } m \text{ near } m_1) \quad (\text{S37})$$

in the transformed variable $\tilde{E}_m = (-1)^m E_m$, where we have defined $\tilde{a}(z) = -a(z)$. Repeating the same analysis as before, we arrive at the odd stopband potential

$$\tilde{V}(z) = \tilde{a}(z) - 2 = -a(z) - 2 \quad (\text{S33})$$

which is plotted in the main text.

We therefore conclude that stopbands in adiabatically chirped photonic crystals are analogous to the classically forbidden regions on a one-dimensional tight-binding quantum chain, with light scattering from the former corresponding to quantum tunneling through the latter.

for some $\alpha_1 > 0$ determined by a_m , or equivalently

$$E_{m+1}^+ = \frac{2\nu}{x} E_m^+ - E_{m-1}^+ \quad (\text{for } m \text{ near } m_1) \quad (\text{S38})$$

where we have defined $\nu \equiv x + (m - m_1)$ and $x \equiv 2/\alpha_1$. In terms of the variables ν and x , the solution to this recurrence is a linear combination of the Bessel functions $E_m^+ = aJ_\nu(x) + bY_\nu(x)$. Now, the asymptotic expansions of the Bessel functions $J_\nu(x)$ and $Y_\nu(x)$ for large argument x (consistent with small α_1 and hence slow chirp) and large order ν (consistent with m far from m_1) depend on the relative magnitude of x and ν . In each case, the asymptotic expansions are given by (see [39], 9.3.2 and 9.3.3):

$$J_\nu(x) \approx \begin{cases} \sqrt{\frac{2}{\pi}} (x^2 - \nu^2)^{-1/4} \cos \left[-\nu \cos^{-1} \left(\frac{\nu}{x} \right) + \sqrt{x^2 - \nu^2} - \frac{\pi}{4} \right] & (\nu < x) \\ \sqrt{\frac{1}{2\pi}} (\nu^2 - x^2)^{-1/4} \exp \left[-\nu \cosh^{-1} \left(\frac{\nu}{x} \right) + \sqrt{\nu^2 - x^2} \right] & (\nu > x) \end{cases} \quad (\text{S39})$$

$$Y_\nu(x) \approx \begin{cases} \sqrt{\frac{2}{\pi}} (x^2 - \nu^2)^{-1/4} \sin \left[-\nu \cos^{-1} \left(\frac{\nu}{x} \right) + \sqrt{x^2 - \nu^2} - \frac{\pi}{4} \right] & (\nu < x) \\ -\sqrt{\frac{2}{\pi}} (\nu^2 - x^2)^{-1/4} \exp \left[\nu \cosh^{-1} \left(\frac{\nu}{x} \right) - \sqrt{\nu^2 - x^2} \right] & (\nu > x) \end{cases} \quad (\text{S40})$$

We can then express these Bessel function expansions in terms of the original variables m , m_1 , and α by noting $(\nu^2 - x^2) = (a_m^2 - 4)/\alpha_1^2$ in the linearized region and applying the change of variable $k \rightarrow k + m_1 - x$ to obtain

$$\nu \cos^{-1} \left(\frac{\nu}{x} \right) - \sqrt{x^2 - \nu^2} = \int_\nu^x \cos^{-1} \left(\frac{k}{x} \right) dk = \int_m^{m_1} \cos^{-1} \left(\frac{a_k}{2} \right) dk \quad (\text{S41})$$

$$\nu \cosh^{-1} \left(\frac{\nu}{x} \right) - \sqrt{\nu^2 - x^2} = \int_x^\nu \cosh^{-1} \left(\frac{k}{x} \right) dk = \int_{m_1}^m \cosh^{-1} \left(\frac{a_k}{2} \right) dk \quad (\text{S42})$$

Combining these results, the Bessel function asymptotic expansions can be rewritten as

$$J_\nu(x) \approx \begin{cases} \sqrt{\frac{2\alpha_1}{\pi}} (4 - a_m^2)^{-1/4} \cos \left[-\int_m^{m_1} \cos^{-1} \left(\frac{a_k}{2} \right) dk - \frac{\pi}{4} \right] & (m < m_1) \\ \sqrt{\frac{\alpha_1}{2\pi}} (a_m^2 - 4)^{-1/4} \exp \left[-\int_{m_1}^m \cosh^{-1} \left(\frac{a_k}{2} \right) dk \right] & (m > m_1) \end{cases} \quad (\text{S43})$$

$$Y_\nu(x) \approx \begin{cases} \sqrt{\frac{2\alpha_1}{\pi}} (4 - a_m^2)^{-1/4} \sin \left[-\int_m^{m_1} \cos^{-1} \left(\frac{a_k}{2} \right) dk - \frac{\pi}{4} \right] & (m < m_1) \\ -\sqrt{\frac{2\alpha_1}{\pi}} (a_m^2 - 4)^{-1/4} \exp \left[\int_{m_1}^m \cosh^{-1} \left(\frac{a_k}{2} \right) dk \right] & (m > m_1) \end{cases} \quad (\text{S44})$$

so that the linear combination of Bessel functions $E_m^+ = aJ_\nu(x) + bY_\nu(x)$ therefore becomes

$$E_m^+ = \begin{cases} \frac{1}{\sqrt[4]{4 - a_m^2}} \left[\sqrt{\frac{\alpha_1}{2\pi}} (ae^{i\pi/4} - be^{-i\pi/4}) \exp \left\{ i \int_m^{m_1} \cos^{-1} \left(\frac{a_k}{2} \right) dk \right\} + \text{C.C.} \right] & (m < m_1) \\ \frac{1}{\sqrt[4]{a_m^2 - 4}} \left[-b \sqrt{\frac{2\alpha_1}{\pi}} \exp \left\{ \int_{m_1}^m \cosh^{-1} \left(\frac{a_k}{2} \right) dk \right\} + a \sqrt{\frac{\alpha_1}{2\pi}} \exp \left\{ -\int_{m_1}^m \cosh^{-1} \left(\frac{a_k}{2} \right) dk \right\} \right] & (m > m_1) \end{cases} \quad (\text{S45})$$

as our asymptotic solution for the field E_m^+ near the turning point m_1 . Comparing this result with the relevant regions of our discrete WKB solution (S36) and eliminating the intermediate coefficients a and b yields

$$\begin{aligned} A &= e^{-i\pi/4} \left(\frac{C}{2} + iD \right) \\ B &= e^{+i\pi/4} \left(\frac{C}{2} - iD \right) \end{aligned} \quad (\text{S46})$$

These are the matching relations across the $m = m_1$ turning point.

2. Matching Across Even $m = m_2$ Turning Point

We define the even stopband tunneling parameter

$$\gamma = \int_{m_1}^{m_2} \cosh^{-1} \left(\frac{a_m}{2} \right) dm. \quad (\text{S47})$$

Using γ , we can then rewrite the discrete WKB solution (S36) as

$$E_m^+ = \begin{cases} \frac{1}{\sqrt[4]{4 - a_m^2}} \left[A \exp \left\{ i \int_m^{m_1} \cos^{-1} \left(\frac{a_k}{2} \right) dk \right\} + B \exp \left\{ -i \int_m^{m_1} \cos^{-1} \left(\frac{a_k}{2} \right) dk \right\} \right] & (m < m_1) \\ \frac{1}{\sqrt[4]{a_m^2 - 4}} \left[D e^{-\gamma} \exp \left\{ \int_m^{m_2} \cosh^{-1} \left(\frac{a_k}{2} \right) dk \right\} + C e^{\gamma} \exp \left\{ - \int_m^{m_2} \cosh^{-1} \left(\frac{a_k}{2} \right) dk \right\} \right] & (m_1 < m < m_2) \\ \frac{1}{\sqrt[4]{4 - a_m^2}} \left[F \exp \left\{ -i \int_m^{m_2} \cos^{-1} \left(\frac{a_k}{2} \right) dk \right\} + G \exp \left\{ i \int_m^{m_2} \cos^{-1} \left(\frac{a_k}{2} \right) dk \right\} \right] & (m_2 < m) \end{cases} \quad (\text{S48})$$

This reformulation is useful for matching near $m = m_2$, since the discrete WKB solution in the stopband is now expressed as a function of right turning point m_2 . The recurrence (S12) linearized near $m = m_2$ takes the form

$$E_{m+1}^+ = [2 - \alpha_2 (m - m_2)] E_m^+ - E_{m-1}^+ \quad (\text{for } m \text{ near } m_2) \quad (\text{S49})$$

or equivalently,

$$\tilde{E}_{m+1}^+ = \frac{2\nu}{x} \tilde{E}_m^+ - \tilde{E}_{m-1}^+ \quad (\text{S50})$$

where we have defined $\nu \equiv x - (m - m_2)$ and $x \equiv 2/\alpha_2$. In terms of the variables ν and x , the solution to this recurrence is a linear combination of the Bessel functions $E_m^+ = aJ_\nu(x) + bY_\nu(x)$, just as in the $m = m_1$ case. In particular, the mapping from the $m = m_1$ case is exact under the switch $m \leftrightarrow m_1$ (so as to obtain the modified m -dependence of ν) and subsequent replacements $m_1, \alpha_1 \rightarrow m_2, \alpha_2$. Applying this transformation to the linear combination of asymptotic Bessel functions (S45) gives

$$E_m^+ = \begin{cases} \frac{1}{\sqrt[4]{4 - a_m^2}} \left[\sqrt{\frac{\alpha_2}{2\pi}} (ae^{i\pi/4} - be^{-i\pi/4}) \exp \left\{ i \int_m^{m_2} \cos^{-1} \left(\frac{a_k}{2} \right) dk \right\} + \text{C.C.} \right] & (m_2 < m) \\ \frac{1}{\sqrt[4]{a_m^2 - 4}} \left[-b\sqrt{\frac{2\alpha_2}{\pi}} \exp \left\{ \int_m^{m_2} \cosh^{-1} \left(\frac{a_k}{2} \right) dk \right\} + a\sqrt{\frac{\alpha_2}{2\pi}} \exp \left\{ - \int_m^{m_2} \cosh^{-1} \left(\frac{a_k}{2} \right) dk \right\} \right] & (m_2 > m) \end{cases} \quad (\text{S51})$$

as the asymptotic solution for the field E_m^+ near the turning point m_2 . Comparing this result with the relevant regions of our discrete WKB solution (S48) and eliminating the intermediate coefficients a and b yields

$$\begin{aligned} F &= e^{-i\pi/4} \left(C e^{\gamma} + \frac{iD}{2} e^{-\gamma} \right) \\ G &= e^{+i\pi/4} \left(C e^{\gamma} - \frac{iD}{2} e^{-\gamma} \right) \end{aligned} \quad (\text{S52})$$

These are the matching relations across the $m = m_2$ turning point.

3. Matching Across Entire Even Stopband

Eliminating the coefficients C and D in the matching relations (S46) and (S52) finally gives

$$\begin{aligned} A &= \left(e^{\gamma} + \frac{1}{4} e^{-\gamma} \right) F + i \left(e^{\gamma} - \frac{1}{4} e^{-\gamma} \right) G \\ B &= -i \left(e^{\gamma} - \frac{1}{4} e^{-\gamma} \right) F + \left(e^{\gamma} + \frac{1}{4} e^{-\gamma} \right) G \end{aligned} \quad (\text{S53})$$

These are the discrete WKB connection formulae across an entire $a_m > 2$ stopband and are identical to the connection formulae across a potential barrier in the standard, continuous WKB approximation [27].

B. Odd Stopband Connection Formulae

Now consider an $a_m < -2$ stopband for $m \in [m_1, m_2]$ (where m_1, m_2 are not necessarily integers), surrounded on either side by propagation bands $|a_m| < 2$. We can transform the solution E_m^+ in this odd stopband region, given again by Eq. (S36), to a solution in the region near an even stopband by taking

$$\begin{aligned} a_m &\rightarrow \tilde{a}_m \equiv -a_m \\ E_m^+ &\rightarrow \tilde{E}_m^+ \equiv (-1)^m E_m^+ \end{aligned} \quad (\text{S54})$$

which leaves the recursion relation (S12) unchanged. This transformation can be achieved by multiplying (S36) by $(-1)^m$ and using the identities $\cos^{-1}(a_m/2) = \pi - \cos^{-1}(\tilde{a}_m/2)$ and $(-1)^m e^{\pm im\pi} = 1$. Effecting this transformation yields

$$\tilde{E}_m^+ = \begin{cases} \frac{1}{\sqrt[4]{4 - \tilde{a}_m^2}} \left[\tilde{A} \exp \left\{ i \int_{m_1}^{m_2} \cos^{-1} \left(\frac{\tilde{a}_k}{2} \right) dk \right\} + \tilde{B} \exp \left\{ -i \int_{m_1}^{m_2} \cos^{-1} \left(\frac{\tilde{a}_k}{2} \right) dk \right\} \right] & (m < m_1) \\ \frac{1}{\sqrt[4]{4 - \tilde{a}_m^2}} \left[\tilde{F} \exp \left\{ -i \int_{m_2}^m \cos^{-1} \left(\frac{\tilde{a}_k}{2} \right) dk \right\} + \tilde{G} \exp \left\{ i \int_{m_2}^m \cos^{-1} \left(\frac{\tilde{a}_k}{2} \right) dk \right\} \right] & (m_2 < m) \end{cases} \quad (\text{S55})$$

where we have defined

$$\begin{aligned} \tilde{A} &= e^{-im_1\pi} B \\ \tilde{B} &= e^{+im_1\pi} A \\ \tilde{F} &= e^{-im_2\pi} G \\ \tilde{G} &= e^{+im_2\pi} F \end{aligned} \quad (\text{S56})$$

Since the transformed variable \tilde{a}_m describes an even $\tilde{a}_m \equiv -a_m > 2$ stopband, we can apply the even stopband connection formulae (S53) to the transformed discrete WKB solution (S55) and match the transformed coefficients $\tilde{A}, \dots, \tilde{G}$. Applying this even stopband matching and subsequently transforming back to the original coefficients A, \dots, G finally gives

$$\begin{aligned} B &= e^{+im_1\pi} \left[e^{-im_2\pi} \left(e^\gamma + \frac{1}{4} e^{-\gamma} \right) G + i e^{+im_2\pi} \left(e^\gamma - \frac{1}{4} e^{-\gamma} \right) F \right] \\ A &= e^{-im_1\pi} \left[-i e^{-im_2\pi} \left(e^\gamma - \frac{1}{4} e^{-\gamma} \right) G + e^{+im_2\pi} \left(e^\gamma + \frac{1}{4} e^{-\gamma} \right) F \right] \end{aligned} \quad (\text{S57})$$

where

$$\gamma = \int_{m_1}^{m_2} \cosh^{-1} \left(\frac{\tilde{a}_m}{2} \right) dm = \int_{m_1}^{m_2} \cosh^{-1} \left(-\frac{a_m}{2} \right) dm. \quad (\text{S58})$$

These are the discrete WKB connection formulae across an entire odd stopband and are precisely the relations contained in Eq. (S14). Interestingly, odd stopbands have no analogy in the continuous WKB approximation, and the odd stopband connection formulae (S14) are not identical to the even stopband/continuous WKB connection formulae (S53). In particular, the presence of additional turning point phases $\exp(\pm im_{1,2}\pi)$ in the odd stopband connection formulae (S57) has important consequences in quantum mechanical applications [26].

IV. TEM IMAGE ANALYSIS

In the main text, we compare the bilayer number N found in several ACPCs in nature to our predicted minimal number of bilayers $N_{\text{exp/lin}}^{\gamma \sim 1}$ in the case of exponential and linear chirp. This comparison requires an estimate of the optical thickness ratio

$$\Xi = (\ell_L)_m / (\ell_H)_m = n_L (d_L)_m / n_H (d_H)_m, \quad (\text{S59})$$

which we estimate for each biological ACPC via analysis of TEM images given in the relevant reference. In this section we detail the image analysis process, a sketch of which is shown in Fig. S1, using the elytra of the golden *Chrysina aurigans* beetle [28] as an example.

First, an anisotropic Gaussian filter is applied to the TEM image along the assumed axis of the ACPC, which smooths the image while highlighting the low- and high-index layers. Then a curvature flow filter is applied in order further smooth the image while preserving the edges between low- and high-index layers. Finally we binarize the image, where the binarization thresholds are determined locally in the image in order to isolate the low- and high-index layers.

After binarization, we take a thin (few pixel high) horizontal cross-section of the image, from which the layer thicknesses $(d_{L/H})_m$ and hence local optical thickness ratios Ξ_m (S59) can be determined. The value of Ξ_m for each bilayer m in the *C. aurigans* TEM image is plotted in Fig. S2. The fixed ratio Ξ is finally estimated by taking the average optical thickness ratio $\Xi = \mu_{\Xi}$ over all the ACPC bilayers m .

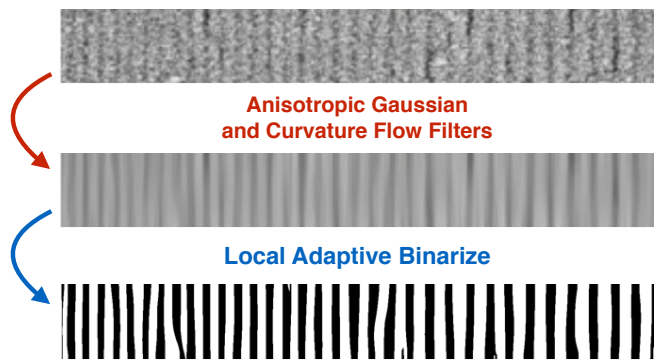


FIG. S1. Sketch of our TEM image analysis procedure applied to the ACPC in the elytra of the golden *C. aurigans* beetle. Original TEM image (top) taken from Ref. [28].

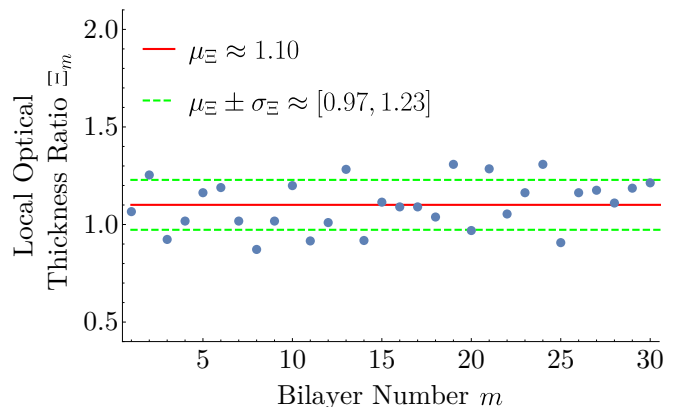


FIG. S2. Plot of the local optical thickness ratios Ξ_m calculated for each bilayer m in the *C. aurigans* TEM image shown in Fig. S1. The Ξ_m values for the first and last measured bilayers are discarded to account for possible incomplete cropping of the original TEM image. The mean optical thickness ratio μ_{Ξ} and the standard deviations $\mu_{\Xi} \pm \sigma_{\Xi}$ about the mean are also shown.